Xue-Ting Ren, Ying Yang*, Yi-Ping Wang and Peng-Xiao Nie

Crystal Structures and Properties of $Pb(Ni_{1/3},Nb_{2/3})O_3$–$Pb(Zr_{1/2},Ti_{1/2})O_3$ Thin Films on Silicon Substrates

DOI 10.1515/ehs-2014-0053

Abstract: $Pb(Zr,Ti)O_3$ (PZT)-based ternary system thin films, xPb(Ni,Nb)O_3–(1–x)PZT (50/50) (PNN–PZT), are grown on $Pt/TiO_2/SiO_2/Si$ substrates using radio-frequency magnetron sputtering system. The intrinsic PZT (50/50) thin films are also deposited for comparison. XRD data display a perovskite structure in PNN–PZT thin films, which is similar with that of PZT films. On the other hand, the adding of PNN induces a change in the ratio of (200)/(002) peak intensity in the diffraction patterns, and the tetragonality of PNN–PZT thin films decreases with increasing x. The morphotropic phase boundary (MPB) of PNN–PZT thin film system is confirmed near the composition of 0.05PNN–0.95PZT. PNN–PZT thin films exhibit excellent piezoelectricity and ferroelectricity which are distinctly better than those of PZT thin films. In particular, very high remanent polarization, $P_r = 99$ μC/cm^2, small coercive field of 55 kV/cm, large relative dielectric constants, $\varepsilon_r = 2{,}030$ and distinct piezoelectric response are observed from sample 0.05PNN–0.95PZT.

Keywords: dielectric property, ferroelectricity, PNN–PZT thin films, piezoelectric response

***Corresponding author: Ying Yang,** State Key Laboratory of Mechanics and Control of Mechanical Structures, Nanjing University of Aeronautics and Astronautics, Nanjing 210016, China, E-mail: yingyang@nuaa.edu.cn
Xue-Ting Ren, College of Materials Science and Technology, Nanjing University of Aeronautics and Astronautics, Nanjing 210016, China; State Key Laboratory of Mechanics and Control of Mechanical Structures, Nanjing University of Aeronautics and Astronautics, Nanjing 210016, China, E-mail: rxtzyp@163.com
Yi-Ping Wang, State Key Laboratory of Mechanics and Control of Mechanical Structures, Nanjing University of Aeronautics and Astronautics, Nanjing 210016, China, E-mail: yipingwang@nuaa.edu.cn
Peng-Xiao Nie, College of Materials Science and Technology, Nanjing University of Aeronautics and Astronautics, Nanjing 210016, China; State Key Laboratory of Mechanics and Control of Mechanical Structures, Nanjing University of Aeronautics and Astronautics, Nanjing 210016, China, E-mail: pengxiaonie@nuaa.edu.cn

Introduction

$Pb(Zr,Ti)O_3$ (PZT)-based perovskites are well known for their useful functionality, including piezoelectricity, ferroelectricity and pyroelectricity. In recent years, ferroelectric thin films have been used for broad applications ranging from nonvolatile memory storage devices, microactuators, microsensors and micro-electro-mechanical systems (MEMS) (Kim, Koo, and Lee 2011; Zhang, Wasa, and Zhang 2009; Xu, Trolier-McKinstry, and Ren 2001). PZT-based ternary perovskite ceramics, PZT with relaxors additive such as $Pb(Mg,Nb)O_3$(PMgN) and $Pb(Mn,Nb)O_3$(PMnN) are researched as functional ceramics, since the additives modify their dielectric and piezoelectric response (Yoon and Jang 1995). Thin films of the PZT-based ternary perovskite could be useful for a production of thin film precise piezoelectric devices. Several approaches have been used for the fabrication of PZT-based thin films, including sputtering, pulsed laser deposition, chemical solution processes and chemical vapor deposition (Uchino 2010). Most of the PZT-based thin films such as PMgN-PZT and PMnN-PZT have been fabricated in polycrystalline structure on nonepitaxial substrates like silicon or in single crystal structure by a heteroepitaxial growth process on MgO or $SrTiO_3$ (STO) single-crystal substrates (Wasa, Kitabatake, and Adachi 2004; Wasa, Kanno, and Kotera 2008; Kanno, Kotera, and Wasa 2003; Wasa, Adachi, and Nishida 2012). The piezoelectric materials of $Pb(Ni_{1/3}Nb_{2/3})O_3$ (PNN)–PZT solid solution also could be formed with relaxor ferroelectric PNN and normal ferroelectric PZT in proper proportion, as these solid solution systems of PMgN-PZT or PMnN-PZT. The ceramic materials have been researched intensively on the phase structures, piezoelectric and dielectric properties (Moulson and Herbert 2003; Lee, Yoon, and Lee 2004; Vittayakorn, Rujijanagul, and Tan 2004; Yoon and Jang 1995). However, few investigations have been reported on the PZT thin films with relaxor additive of PNN. It is then interesting and useful to study the phase structures and piezoelectricity of PNN–PZT thin films (Ruangchalermwong, Li, and Zhu 2009, Chang, Yu, and Dong 2002).

In this work, xPNN–(1–x)PZT ($x = 0$, 0.05, 0.1, 0.15) solid-solution thin films are deposited on $Pt(111)/TiO_2/$

SiO_2/Si by radio-frequency (Rf) magnetron sputtering system. Their crystal structure, ferroelectric properties and piezoelectric response are discussed for potential applications.

Experimental Procedure

Ternary perovskite xPNN–(1–x)PZT (x = 0, 0.05, 0.1, 0.15) thin films were deposited on (111)-Pt/TiO_2/SiO_2/Si substrates by Rf magnetron sputtering system. Meanwhile, PZT(52/48) is near morphotropic phase boundary (MPB) and the adding of PNN shifts the MPB composition slightly to Ti-rich composition. Thus in the researched ternary PNN–PZT films, PZT (50/50) was selected. In film sputtering, the mixed powder target of xPNN– (1–x)PZT composition was composed of the mixture of $PbTiO_3$, $PbZrO_3$, PbO, Nb_2O_5, NiO, where 10% excess PbO in target was used to compensate the likely loss of this volatile component during thin film preparation. The substrate temperature is 600°C, the Rf-power is fixed at 100 W, the distance between the target and substrate is 4 cm. The gas pressure of PNN–PZT thin films is maintained at 0.5 Pa ($Ar/O_2 = 20/0$), while, the growth atmosphere of the intrinsic PZT thin film for comparison is $Ar/O_2 = 20/1$ and the pressure is also 0.5 Pa. Then, the sputtered films are cooled down to room temperature with a rate of 15°C/min in air. These samples are named as 0.05PNN–0.95PZT/Pt, 0.1PNN–0.9PZT/Pt, 0.15PNN–0.85PZT/Pt, PZT/Pt.

The crystal structure of the samples was examined by X-ray diffraction (XRD, Bruker D8 Advance). The cross section of these samples was observed by a field-emission scanning electric microscope (Model Quanta 200, FEI Company). Their surface texture and film morphologies were characterized using atomic force microscopy (AFM, Bruker multimode 8) with an open-loop controller. Meanwhile, the piezoelectric and ferroelectric switching properties of the film were examined using piezoelectric force microscopy (PFM) at the same part of the sample. Conductive Pt–Ti-coated silicon cantilevers were used for PFM imaging and polarization switching studies. Ferroelectric phase/amplitude hysteresis loops versus tip bias were measured in fixed locations on the ferroelectric film surface as a function of a dc switching bias superimposed on the ac modulation bias.

Results and Discussions

Perovskite phase formation, crystal structure and lattice parameter were determined by XRD at room temperature as a function of x. Figure 1(a) shows the XRD patterns of thin films in xPNN–(1–x)PZT system with a well-crystallized perovskite structure for all compositions. Thin films for all compositions in PNN–PZT system do not have impurity phases and pyrochlore phase compared to the PZT thin film. They have almost similar XRD spectrum to that of the intrinsic PZT films, both exhibit perovskite structure. Diffraction peaks could be indexed as crystal structure by considering the obvious splitting or broadening of the (200)/(002) signals in Figure 1(a). In order to clarify the phase structure more accurately, the amplified image of (200) and (002) diffraction peaks was shown in Figure 1(b). The data illustrate that (200) and (002) peaks split in the diffraction pattern of PZT (50/50) film; this is understood that the selected composition is near the morphotropic phase boundary, in which the rhombohedral and tetragonal phases coexist. The split of (200)/(002) peaks takes place in the tetragonal phase. From the ratio of (200)/(002) peaks intensity, it could be seen qualitatively there is more tetragonal phase in the deposited PZT (50/50) film. With the increasing of x, the ratio of (200)/(002) peaks intensity increases, indicating the increasing of rhombohedral phase in PNN–PZT thin films. This variation in the relative intensity of (200) and (002) diffraction peaks has been also observed the previous research in PNN–PZT ceramics, where the adding of PNN induces the crystal structure turning to rhombohedral phase (Yuan, Yang, and Hu 2014). However, in the reported PNN–Pb($Zr_{0.5}Ti_{0.5}$)O_3 system, the MPB composition has been confirmed at 0.15–0.2 PNN–PZT. In this deposited PNN–PZT films, the MPB composition is 0.05PNN–0.95PZT. The reason that the MPB of PNN–PZT thin films is different from ceramics could be complicated from these effects of internal stress, grain size, textural growth and so on. The lattice parameters of both films and the bulk PZT (50/50) ceramics were listed in

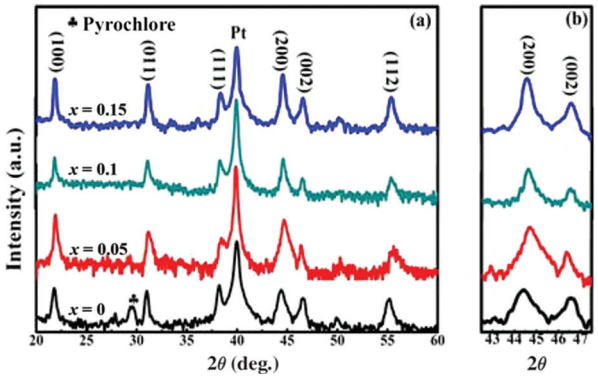

Figure 1: XRD patterns of (a) xPNN–(1–x)PZT thin films grown on (111)-Pt/TiO_2/SiO_2/Si substrates and (b) the amplified image of (002) and (200) diffraction peaks.

Table 1: Lattice constants and c/a ratios of PZT-based materials.

Materials	c-axis (Å)	a-axis (Å)	c/a ratios
PNN–PZT[a]	4.066	4.051	1.003
PZT[a]	4.081	4.066	1.004
PZT[b]	4.147	4.032	1.029

Note: [a]Film; [b]bulk materials (Zhang, Wasa, and Zhang 2009).

Table 1, which show that the lattice constant c of PZT films is smaller and a is larger than that of bulk PZT (50/50) ceramics, so there is remarkable compressive stresses in c-axis direction. The decrease of c/a indicates the decrease of tetragonality of the structure, which is beneficial to rhombohedral phase. This compressive stress may be the reason of the MPB shift from 0.15–0.2 PNN–PZT in ceramic to 0.05PNN–0.95PZT in thin film.

The cross section of xPNN–(1–x)PZT films is observed by scanning electron microscope, which are shown in Figure 2. All cross-sectional views show dense columnar structures, and the interfaces between thin film and substrate layers are quite clear and sharp, implying little interface reaction and diffusion during film deposition at 600°C substrate temperature. These films thickness under the set deposition parameters is confirmed about 400 nm from the cross-sectional micrographs. It is also found that the thickness of 0.05PNN–0.95PZT thin film is a little larger, which may be induced by the uneven thin films.

Figure 3 shows the polarization–electric field (P–E) hysteresis loops measured at 20 Hz for xPNN–(1–x)PZT films. It is found that the saturated polarization (P_s) and remanent polarization (P_r) values enhanced first, and then decreased with the addition of PNN, as shown in Table 2. The hysteresis curve shows optimal ferroelectric properties with highest P_s of 124 μC/cm^2, P_r of 99 μC/cm^2 and small

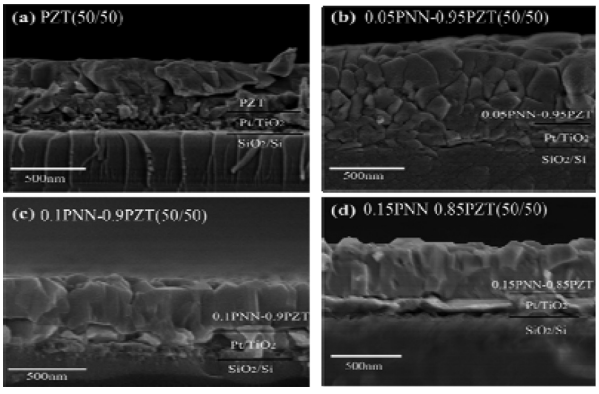

Figure 2: SEM micrographs of cross sections for xPNN– (1–x)PZT films deposited on Pt/TiO_2/SiO_2/Si substrates.

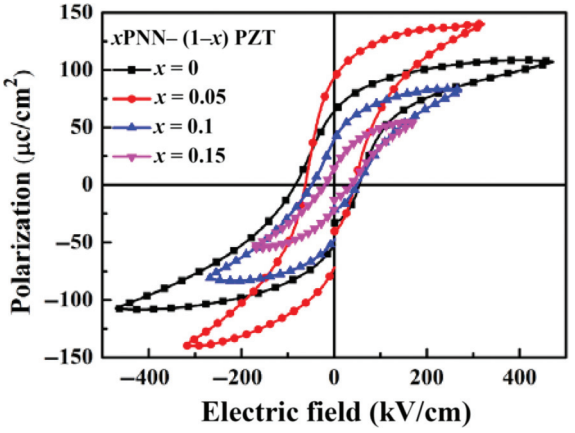

Figure 3: Ferroelectric polarization hysteresis loops of xPNN–(1–x) PZT films at 20 Hz.

Table 2: Characterization of PZT-based film.

Film	ε_r	P_r (C/cm^2) (10^{-6})	P_s (C/cm^2) (10^{-6})	$2E_c$ (V/cm) (10^3)
0.15PNN–0.85PZT	1,470	15.4	54.7	58
0.1PNN–0.9PZT	1,850	39.9	65.5	100
0.05PNN–0.95PZT	2,030	99.1	124	115
PZT	635	64.2	102	150

coercive field ($2E_c$) values of 115 kV/cm at $x = 0.05$, which is near the MPB of PNN–PZT thin films system. With the increase of x, the relative dielectric constant (ε_r) also follows similar variation with that of P_s and P_r. However, compared with PZT and PMnN–PZT films deposited on Pt/TiO_2/SiO_2/Si with dielectric constants of 600–900, the ε_r of PNN–PZT films are much larger.

The microscopic polarization reverse of PZT (50/50) film is presented in Figure 4. Figure 4(a) shows the 5×5 μm^2 topography AFM image of the film surface. No particulates and cracks were observed on the top surface of the film. The grain size and the root mean square (RMS) surface roughness of the deposited film are approximately 150 and 25.8 nm, respectively. The polarization switching was carried out by applying a small dc voltage of −8 V through the PFM tip in contact with the out-of-plane (OP) film surface, imaging a 5×5 μm^2 area, and then switching a square pattern of 3×3 μm^2 area inside the 5×5 μm^2 poled area with +8 V dc voltages. As shown in Figure 4(b), the area poled under −8 V had a polarization pointing toward substrate (i.e. downward polarization) with brown color, and the area poled with +8 V had a polarization pointing against substrate (i.e. upward polarization) with yellow color. Figure 4(c) showed the in-plane

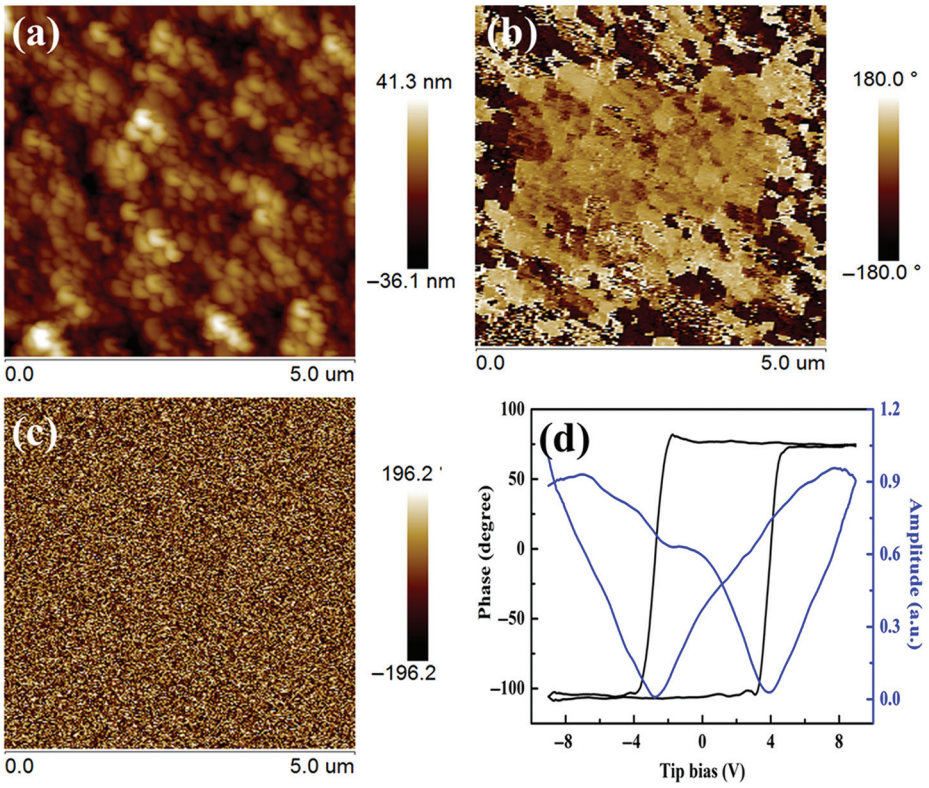

Figure 4: (a) Surface topography, (b) OP-PFM image, (c) IP-PFM image and (d) phase/amplitude voltage hysteresis loops of PZT (50/50) thin film deposited on $Pt/TiO_2/SiO_2/Si$ substrates.

(IP) PFM phase image of the film. It can be seen that the PZT (50/50) film grown on $Pt/TiO_2/SiO_2/Si$ substrates has at least three polarization variants, which could be seen from brown, yellow and white domains. Figure 4(d) shows the phase and amplitude versus tip bias loops of the PZT (50/50) film, which proved its polarization switching and strong piezoelectric response. The phase angle changes also showed that a saturated polarization switching process occurs in PZT (50/50) thin film and the coercive field and butterfly loops were asymmetric.

The smooth surfaces of the films, $10 \times 10\ \mu m^2$ topographies, were shown in Figures 5(a)–7(a). These PNN–PZT solid-solution films were also dense and uniform with no obvious pores, but with bigger grain sizes and rougher surface RMS values. With the increase of x, the grain size grew from 320 to 400 nm, and the RMS increased from approximately 45.5 to 70.4 nm. The microscopic polarization switches of PNN–PZT solid-solution thin films are shown in Figures 5(b), 6(b) and 7(b). The polarization switching was conducted by applying −8 V and +8 V (±0.8 V for 0.1PNN–0.9PZT film in Figure 6(b)) dc voltages on two square patterns of $5 \times 5\ \mu m^2$ and $3 \times 3\ \mu m^2$ areas on the film surface, respectively. Different polarization states and domains display different colors under AFM observation. Comparing these Figures 4(b), 5(b), 6(b) and 7(b), it is found that the film of 0.05PNN–0.95PZT exhibits distinct switch image, implying best ferroelectric polarization switching. As shown in Figure 5(b), the color of the area poled under −8 V is brown and the area poled under +8 V is yellow, indicating downward and upward polarizations. Meanwhile, in the outside unpoled area, tiny dark and yellow dots mix thoroughly, which shows there is no self-polarization taking place in the as-grown polycrystalline 0.05PNN–0.95PZT film. In Figures 5(c), 6(c) and 7(c), two different colors still could be seen in the IP polarization images, signifying two polarization variants and at least two kinds of domains in the polycrystalline PNN–PZT film. Figure 5(d) shows that the phase angle changes, which display a saturated polarization switching and high amplitude piezoelectric response, symmetrical butterfly loops and coercive fields in 0.05PNN–0.95PZT thin film. As the increasing of PNN additive, the phase/amplitude voltage hysteresis loops are then asymmetric, the coercive fields become smaller and the piezoresponse amplitudes become smaller too, as shown in Figures 6(d) and 7(d). This trend complies with the variation in ferroelectric polarization shown in Figure 3.

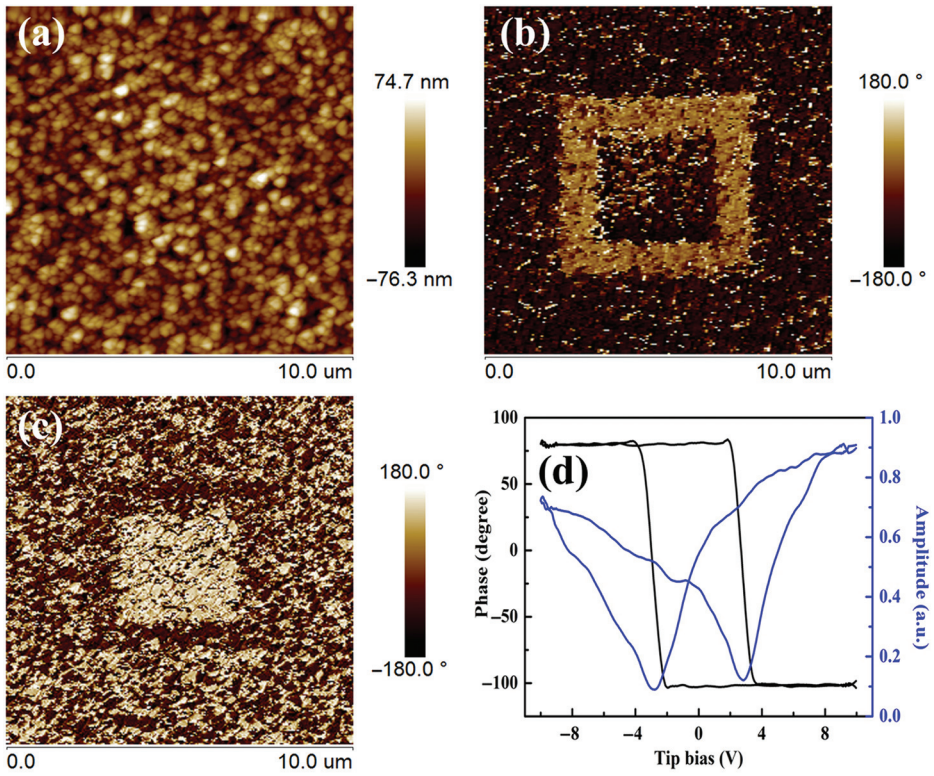

Figure 5: (a) Surface topography, (b) OP-PFM image, (c) IP-PFM image and (d) phase/amplitude voltage hysteresis loops of 0.05PNN–0.95PZT (50/50) thin film deposited on $Pt/TiO_2/SiO_2/Si$ substrates.

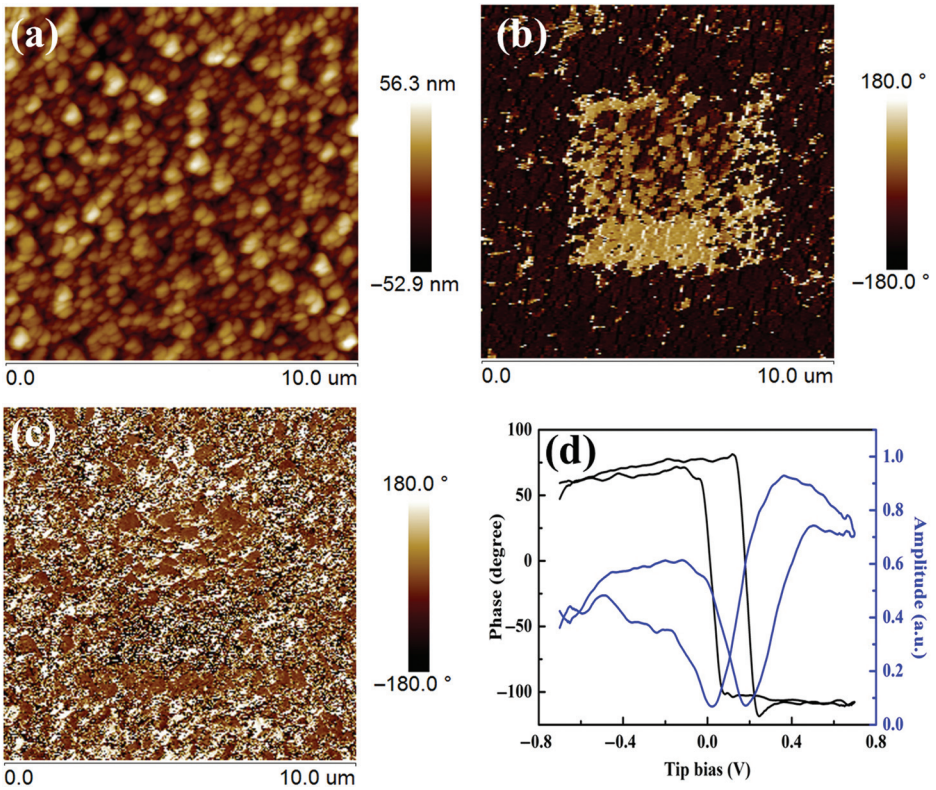

Figure 6: (a) Surface topography, (b) OP-PFM image, (c) IP-PFM image and (d) phase/amplitude voltage hysteresis loops of 0.1PNN–0.9PZT (50/50) thin film deposited on $Pt/TiO_2/SiO_2/Si$ substrates.

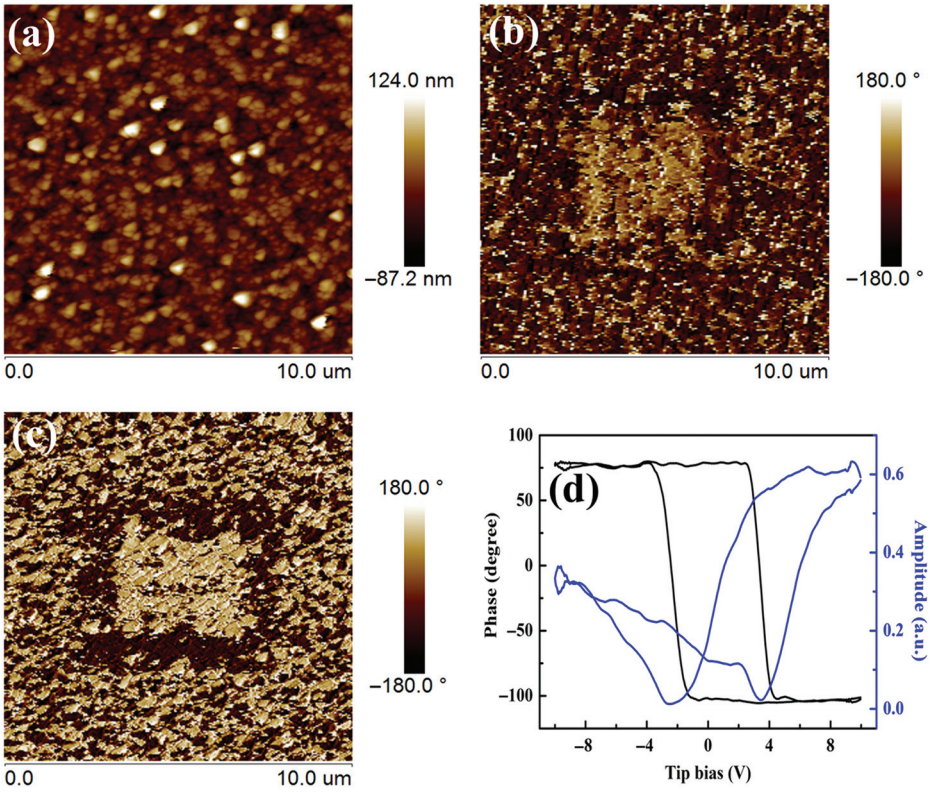

Figure 7: (a) Surface topography, (b) OP-PFM image, (c) IP-PFM image and (d) phase/amplitude voltage hysteresis loops of 0.15PNN–0.85PZT (50/50) thin film deposited on $Pt/TiO_2/SiO_2/Si$ substrates.

Conclusion

In summary, the ternary perovskite PNN–PZT thin films have been successfully deposited on $Pt/TiO_2/SiO_2/Si$ substrates via RF magnetron sputtering system. The PNN–PZT thin films show almost similar crystal structure as that of PZT with perovskite phase, indicating the entire formation of a solid solution. The MPB of the PNN–PZT thin film system is confirmed near 0.05PNN–0.95PZT composition, which is different from the corresponding ceramics. By introducing PNN, the performances of the PZT-based solid-solution films have been largely enhanced. The 0.05PNN–0.95PZT thin film exhibits excellent ferroelectricity with P_r of 99 μC/cm^2, which is better than that of the undoped PZT thin film with MPB composition.

Funding: The work was financially supported by the National Natural Science Foundation of China (No. 11274174), the National Key Project for Basic Research of China (2012CB619406), the 111 project (No. B12021), the Foundation of Graduate Innovation Center in NUAA (No. kfjj201469) and the Fundamental Research Funds for the Central Universities.

References

Chang, H., K. M. Yu, Y. Dong, et al. 2002. "Dielectric Mapping of a Pb $(Ni_{1/3}Nb_{2/3})O_3$-$PbZrO_3$-$PbTiO_3$ Ternary Phase Spread." *Applied Physics Letters* 81 (11):2062–4.

Kanno, I., H. Kotera, K. Wasa, et al. 2003. "Crystallographic Characterization of Epitaxial Pb(Zr, Ti)O_3 Films with Different Zr/Ti Ratio Grown by Radio-Frequency-Magnetron Sputtering." *Journal of Applied Physics* 93 (7):4091–6.

Kim, S. H., C. Y. Koo, J. Lee, et al. 2011. "Enhanced Dielectric and Piezoelectric Properties of Low-Temperature Processed Pb(Zr, Ti)O_3 Thick Films Prepared by Hybrid Deposition Technique with Chemical Solution Infiltration Process." *Materials Letters* 65 (19):3041–3.

Lee, S. M., C. B. Yoon, S. H. Lee, et al. 2004. "Effect of Lead Zinc Niobate Addition on Sintering Behavior and Piezoelectric Properties of Lead Zirconate Titanate Ceramic." *Journal of Materials Research* 19 (09):2553–6.

Moulson, A. J., and J. M. Herbert. 2003. *Electroceramics: Materials, Properties, Applications*. New York: John Wiley & Sons.

Ruangchalermwong, C., J. F. Li, Z. X. Zhu, et al. 2009. "Enhanced Ferro-and Piezoelectric Properties in (100)-Textured Nb-Doped $Pb(Zr_xTi_{1-x})O_3$ Films with Compositions at Morphotropic Phase Boundary." *Thin Solid Films* 517 (24):6599–604.

Uchino, K. 2010. *Advanced Piezoelectric Materials: Science and Technology*. K. Uchino, Ed. Cambridge, UK: Woodhead Publishing, Elsevier.

Vittayakorn, N., G. Rujijanagul, X. Tan, et al. 2004. "The Morphotropic Phase Boundary and Dielectric Properties of the xPb($Zr_{1/2}Ti_{1/2}$)O_3-(1-x)Pb($Ni_{1/3}Nb_{2/3}$)O_3 Perovskite Solid Solution." *Journal of Applied Physics* 96 (9):5103–9.

Wasa, K., H. Adachi, K. Nishida, et al. 2012. "Highly Polarized Single-c-Domain Single-Crystal Pb(Mn, Nb)O_3-PZT Thin Films." *Ultrasonics, Ferroelectrics, and Frequency Control, IEEE Transactions on* 59 (1):6–13.

Wasa, K., I. Kanno, H. Kotera, et al. "Thin Films of PZT-based Ternary Perovskite Compounds for MEMS." In Ultrasonics Symposium, 2008. IUS 2008. IEEE. IEEE, 2008: 213–216.

Wasa, K., M. Kitabatake, and H. Adachi. 2004. *Thin Film Materials Technology: Sputtering of Control Compound Materials*. New York, NY: Springer Science & Business Media.

Xu, F., S. Trolier-McKinstry, W. Ren, et al. 2001. "Domain Wall Motion and Its Contribution to the Dielectric and Piezoelectric Properties of Lead Zirconate Titanate Films." *Journal of Applied Physics* 89 (2):1336–48.

Yoon, M. S., and H. M. Jang. 1995. "Relaxor-Normal Ferroelectric Transition in Tetragonal-Rich Field of Pb($Ni_{1/3}nb_{2/3}$)O_3-$PbTiO_3$-$PbZrO_3$ System." *Journal of Applied Physics* 77 (8):3991–4001.

Yuan, D., Y. Yang, Q. Hu, et al. 2014. "Structures and Properties of Pb($Zr_{0.5}Ti_{0.5}$)O_3-Pb($Zn_{1/3}Nb_{2/3}$)O_3-Pb($Ni_{1/3}Nb_{2/3}$)O_3 Ceramics for Energy Harvesting Devices." *Journal of the American Ceramic Society* 97 (12):3999–4004.

Zhang, T., K. Wasa, S. Zhang, et al. 2009. "High Piezoelectricity of Pb(Zr, Ti)O_3-Based Ternary Compound Thin Films on Silicon Substrates." *Applied Physics Letters* 94 (12):122909.